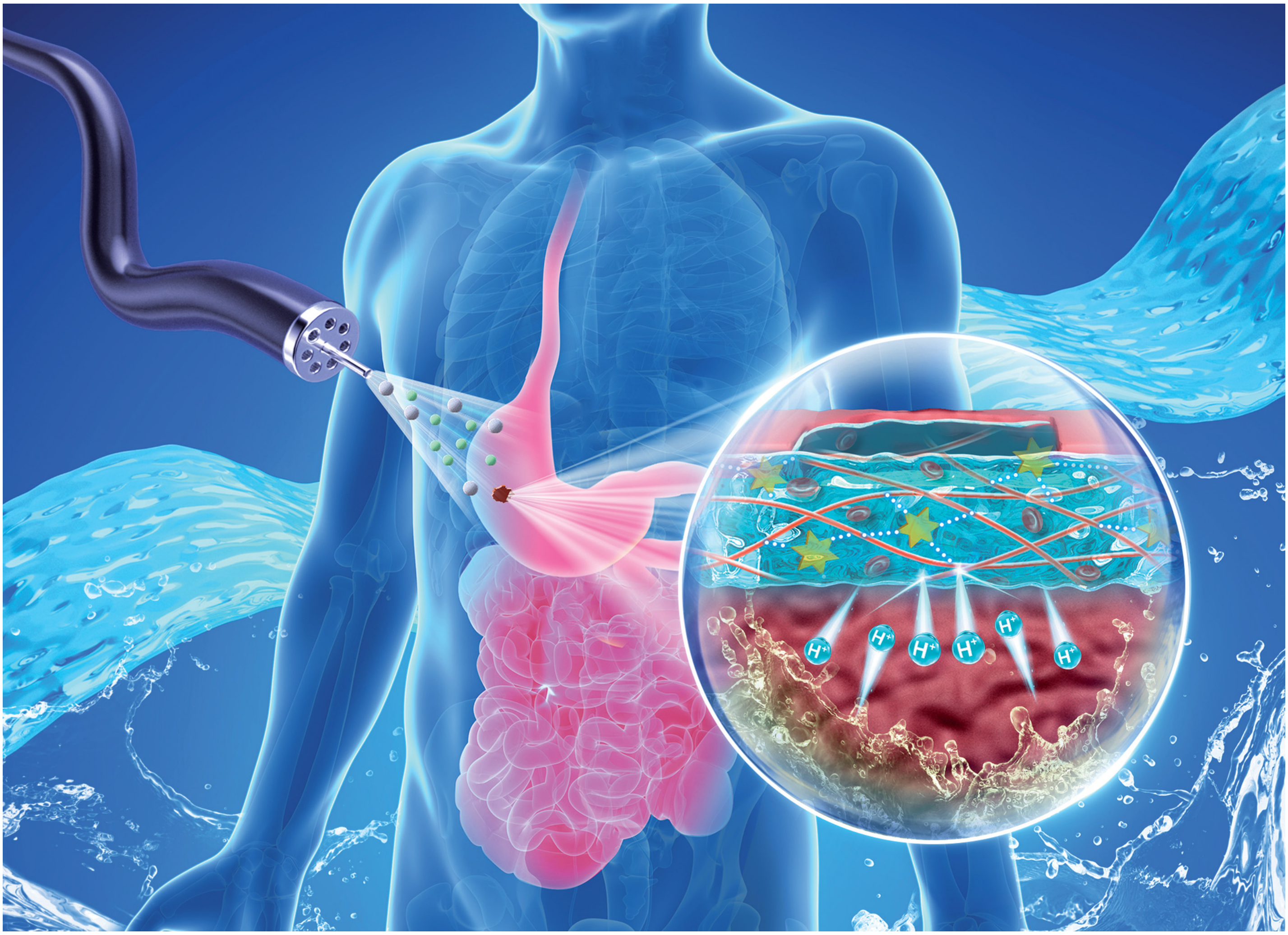

Showcasing research from Professor Rong Wang's laboratory at the Ningbo Institute of Materials Technology and Engineering, Chinese Academy of Sciences, Ningbo, China.

Ionically assembled hemostatic powders with rapid self-gelation, strong acid resistance, and on-demand removability for upper gastrointestinal bleeding

Through ionically assembling *N*-[(2-hydroxy-3-trimethylammonium) propyl] chitosan chloride and phytic acid, hemostatic powders for fast and stable control of upper gastrointestinal bleeding with strong acid resistance and on-demand removability have been developed.

As featured in:

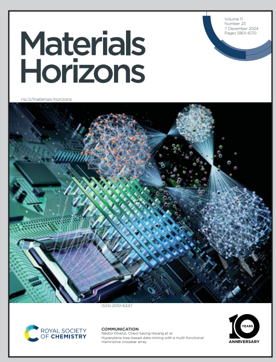

See Rong Wang *et al.*, *Mater. Horiz.*, 2024, **11**, 5983.

Materials Horizons

COMMUNICATION

Cite this: *Mater. Horiz.*, 2024, **11**, 5983

Received 29th June 2024,
Accepted 9th October 2024

DOI: 10.1039/d4mh00837e

rsc.li/materials-horizons

Ionically assembled hemostatic powders with rapid self-gelation, strong acid resistance, and on-demand removability for upper gastrointestinal bleeding†

Ashuang Liu,‡[abc] Zhimao Huang,‡[ab] Shengyong Cui,[d] Ying Xiao,[ab] Xiangshu Guo,[ab] Gaoke Pan,[ab] Lei Song,[ab] Junjie Deng,[abc] Ting Xu,[ab] Youfen Fan[d] and Rong Wang *[ab]

Upper gastrointestinal bleeding (UGIB) is bleeding in the upper part of the gastrointestinal tract with an acidic and dynamic environment that limits the application of conventional hemostatic materials. This study focuses on the development of *N*-[(2-hydroxy-3-trimethylammonium) propyl] chitosan chloride/phytic acid (HTCC/PA, HP) powders with fast hemostatic capability and strong acid resistance, for potential applications in managing UGIB. Upon contact with liquids within 5 seconds, HP powders rapidly transform into hydrogels, forming ionic networks through electrostatic interactions. The ionic crosslinking process facilitates the HP powders with high blood absorption (3.4 times of self-weight), sufficient tissue adhesion (5.2 and 6.1 kPa on porcine skin and stomach, respectively), and hemostasis (within 15 seconds for *in vitro* clotting). Interestingly, the PA imparts the HP powders with strong acid resistance (69.8% mass remaining after 10 days of incubation at pH 1) and on-demand removable sealing while HTCC contributes to fast hemostasis and good wet adhesion. Moreover, the HP powders show good biocompatibility and promote wound healing. Therefore, these characteristics highlight the promising clinical potential of HP powders for effectively managing UGIB.

New concepts

This study demonstrates a new concept of ionic assembly of quaternary polysaccharides and phytic acids (PA) for highly acid-resistant and efficient hemostatic powders. *N*-[(2-hydroxy-3-trimethylammonium) propyl] chitosan chloride (HTCC) and PA are complexed *via* a feasible self-assembling approach to form powders with rapid gelation, fast hemostasis, strong acid resistance, and on-demand removability. It shows great promise for the treatment of upper gastrointestinal bleeding, which is always under extremely acidic and peristaltic working conditions. This ionically assembled HTCC/PA hemostatic powder takes advantage of the efficient deprotonation capability of PA at extremely low pH and the stable but on-demand reversible interactions between quaternary polysaccharides and PA molecules. It is different from the existing polyelectrolyte hemostatic powders, in which the positively charged groups are not balanced and toxic, or the charge density of the complex is prone to be affected by low pH conditions and cannot function properly in the acidic and dynamic upper gastrointestinal environment. This study also provides additional insights into the development of safe and effective materials *via* the novel and feasible ionic assembling approach for biomedical applications.

1. Introduction

Upper gastrointestinal bleeding (UGIB) is bleeding in the upper part of the gastrointestinal system from the oesophagus to the ligament of Treitz, including the oesophagus, stomach, and duodenum. It is one of the most common emergencies in hospitals, with an annual incidence ranging from 40 to 150 per 100 000 patients and an overall mortality rate ranging from 3% to 14%.[1–3] In the United States, 7.6 billion dollars have been spent yearly on UGIB during hospitalization.[4] Endoscopic intervention is still considered the 'gold standard' for the treatment of UGIB. However, the conventional thermal, physical (clips), and pharmacological (injection of epinephrine, sclerosant, or thrombin) approaches are hard to apply to wounds in the upper gastrointestinal (GI) tract that are difficult to visualise, prone to diffuse bleeding, and consist of fragile tissue.[2] Additionally, current treatments have limitations, including a risk of perforation, high technical requirements, and the need for repeat surgeries to remove unabsorbable agents.[5,6] Reoccurrence of UGIB still occurs in 7–16% of all cases and remains remarkably high (20–22%) in patients with

[a] *Laboratory of Advanced Theranostic Materials and Technology, Ningbo Institute of Materials Technology and Engineering, Chinese Academy of Sciences, Ningbo, 315201, P. R. China. E-mail: rong.wang@nimte.ac.cn*
[b] *Zhejiang International Scientific and Technological Cooperative Base of Biomedical Materials and Technology, Ningbo Cixi Institute of Biomedical Engineering, Ningbo, 315300, P. R. China*
[c] *Cixi Biomedical Research Institute, Wenzhou Medical University, Ningbo, 325035, P. R. China*
[d] *Department of Burn Surgery, Ningbo No. 2 Hospital, Ningbo, 315010, P. R. China*

† Electronic supplementary information (ESI) available. See DOI: **https://doi.org/10.1039/d4mh00837e**

‡ A. Liu and Z. Huang contributed equally to this work.

peptic ulcer bleeding.[3] Hemostatic powders have provided a practical strategy that is easy to use, non-traumatic, and able to reach anatomically difficult regions in recent years.[4,7] However, the GI tract, typically the stomach, contains highly acidic stomach acids (pH 1.5–3.5), food bolus, and chyme, and is in a dynamic condition of continuous gastric movement.[8–10] Conventional hemostatic materials, such as fibrin,[11] cellulose,[12] and cyanoacrylate,[13] can hardly satisfy the acidic and peristaltic working environment in the upper GI tract. In addition, the hemostatic materials need to be removable on demand to prevent the excessive adhesion of tissues to other internal surfaces. Therefore, there is an urgent clinical demand for developing hemostatic materials with strong acid resistance, fast hemostasis, sufficient sealing capability, removability with demand, and biocompatibility for UGIB.

The current commercial hemostatic materials for UGIB are mainly hemostatic powders, including chitosan-based (Celox), starch-based (EndoClot), mineral-based (TC-325), and dextran-based (Nexpowder), which can easily be applied to the bleeding site in the GI tract.[14] TC-325 is the most commonly used commercial hemostatic powder for gastrointestinal bleeding. It seals the bleeding site and concentrates coagulation factors for hemostasis. Although TC-325 has a good initial hemostasis rate of 94.5%, the high rebleeding rate due to sloughing and potential injuries caused by the high pressure of CO_2 limits its application.[14,15] EndoClot has similar hemostatic mechanisms as TC-325. It has immediate hemostasis rates of 83–100% and can promote the healing of ulcers. However, EndoClot is absorbed quickly in 24 h and is limited in wounds due to a high rebleeding risk in 3 days. Hydrolysis of the ester and amide bonds of the oxidized dextran/succinic anhydride hydrogel network by stomach acid leads to the failure of Nexpowder and limits its application in the upper GI system.[14] Ionically assembled powders have been reported recently for GI sealing applications. For instance, Peng *et al.* reported a self-gelling polyethyleneimine and polyacrylic acid (PEI/PAA) powder that can physically crosslink as a hydrogel in seconds with strong gastric and intestinal sealing and good hemostasis.[16] However, the PEI/PAA powder is unstable at extremely low pH (pH < 2) due to the change in charge density of the polyelectrolytes. Guo *et al.* developed hybrid dry powders (HDPs) consisting of polycation and polyanion powders. The gelated hydrogels formed by electrostatic interactions provide tolerance in strong acid (pH 1) and stable sealing for wet and dynamic gastric wounds.[17] However, the HDPs exhibit no evidence of hemostasis for UGIB. The chitosan-based materials can aggregate red blood cells, activate platelets, improve clot formation, and promote cell proliferation.[18–20] However, pure chitosan has limitations in wet adhesion and blood uptake. Recent reports show that quaternized chitosan (such as *N*-[(2-hydroxy-3-trimethylammonium) propyl] chitosan chloride, HTCC) improves blood cell adhesion[21–23] and exhibits excellent antibacterial performance[24–26] due to the enhanced positive charges of the quaternary ammonium groups. However, the direct exposure of the quaternary ammonium groups could lead to cell lysis and can hardly form hydrogels in liquids to establish stable sealing on wounds, limiting their biomedical applications.[27,28] The construction of a stable HTCC-based hemostatic powder that retains the superior hemostatic capability of HTCC in a highly acidic environment, while reducing or even eliminating its cytotoxicity would be of great significance due to its good availability, cost-effectiveness, and multiple biofunctionalities. Phytic acid (PA) is a polyphosphate with a snowflake-like structure and widely exists in daily life, such as in nuts, cereals, vegetables, and oils.[29] PA can dissociate six protons even in strongly acidic environments[30,31] to make negatively charged phosphates which facilitate electrostatic interactions with quaternized chitosan, HTCC, through ionic networks. The cytotoxicity of HTCC is expected to be mitigated by balancing the positive charges of quaternary ammonium groups with the negative charges of phosphate groups in PA. The hydrogels are formed through electrostatic interactions between the HTCC and PA molecules, resulting in stable sealing even under strongly acidic conditions. In addition, PA also exhibits excellent antioxidant[32,33] and anti-inflammatory[34–36] activities, which may be potentially beneficial to wound healing.[37,38]

In this study, we reported a novel HTCC/PA (HP) system that balances the strong charges of the positive charges of HTCC and the negative charges of PA *via* feasible ionic crosslinking to construct hemostatic materials for UGIB applications. The complex can establish rapid gelation by absorbing liquids from wound sites to generate hydrogels. The *in situ*-formed hydrogels can withstand strongly acidic environments. Consequently, the HP powders show good wet adhesion on porcine and rat stomachs, establishing stable sealing. Furthermore, the HP powders can form uniform clots within 15 seconds by concentrating coagulation factors, aggregating blood cells, and activating platelets. Thus, the HP powders exhibit excellent hemostatic performance in rat tail and liver bleeding models. Apart from the stable sealing formed on wound sites, the HP powders can be removed on demand by rinsing with salt solutions, which is potentially beneficial to reducing the risk of tissue adhesion after surgery. *In vitro* and *in vivo* studies confirmed that the HP powders have good hemocompatibility, cytocompatibility, and tissue compatibility, thereby enhancing wound healing. Overall, the HP powders exhibit rapid gelation, strong acid resistance, good blood absorption, on-demand removable wet adhesion, and good biocompatibility. These properties satisfy the urgent clinical need for new strategies in managing UGIB.

2. Results and discussion

2.1 Preparation and characterization of HP powders and hydrogels

HP powders were prepared by simply mixing HTCC powder and PA powder at pre-determined weight ratios. Once in contact with liquids, the HP powders rapidly gelled and formed hydrogels within 5 seconds (Fig. 1 and Movie S1, ESI†), which were obtained through ionic crosslinking, facilitated by the electronic interactions between the positively charged groups in HTCC and the negatively charged groups in PA, namely quaternary

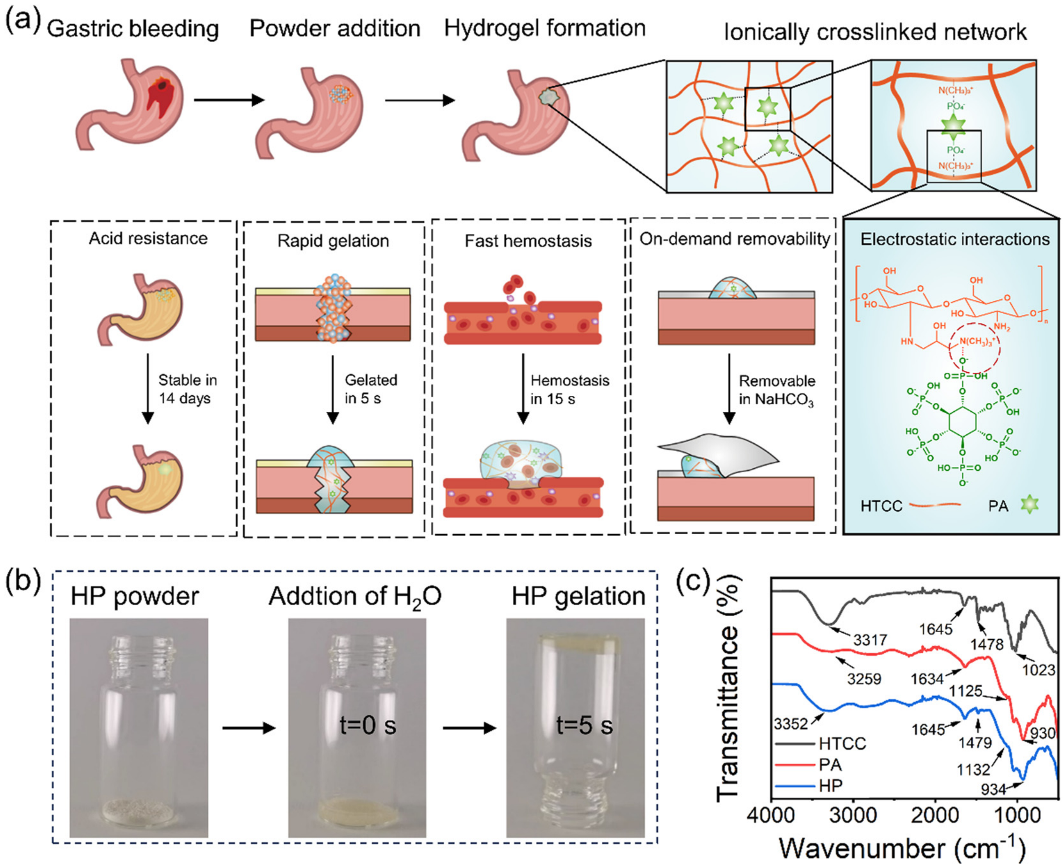

Fig. 1 (a) Schematic illustration of HP powders and *in situ*-formed hydrogels with rapid gelation, acid resistance, fast hemostasis, and removable sealing for treatment of UGIB. Upon contact with liquids, HP powders formed ionically crosslinked networks for gelation. (b) Gelation of HP powder after the addition of water within 5 seconds. (c) FTIR spectra of HTCC, PA, and HP powders.

ammonium groups and phosphate groups, respectively (Fig. 1(a)). The Fourier-transform infrared (FTIR) spectrum indicated that the absorption peaks of HTCC were primarily located at 1023 cm^{-1} (–C–O–), 1645 cm^{-1} (–N–H), and 3317 cm^{-1} (–O–H)[39] (Fig. 1(c)). The characteristic peak of *N*-(2-hydroxypropyl)-3-trimethyl-ammonium groups in HTCC at 1479 cm^{-1} was observed in the HP powders.[26] Additionally, the characteristic absorption peaks of PA at 930 cm^{-1} (P–O–C), 1125 cm^{-1} (P═O), and 1634 cm^{-1} (–O–P–O) appeared for the HP hydrogels as well.[40] No new peak appeared in the HP spectrum, indicating that the formation of the HP hydrogel was mainly *via* physical interactions between HTCC and PA.

The morphology of the HP powders was observed using scanning electron microscopy (SEM). The size of the HTCC and HP powders ranges from 50 μm to 150 μm (Fig. 2(a)). The PA powders were adsorbed on the surfaces of the HTCC powders homogeneously, which could facilitate rapid hydrogel formation after liquid absorption. The obtained HP hydrogel showed great injectability from a syringe (Fig. 2(b)), making it adaptable for application to wounds with various shapes and depths. The optimum HTCC/PA ratio of HP powders was further investigated by evaluating the mechanical properties, stability in acidic environments, and blood absorption capability. The HP hydrogel showed good adhesion on various surfaces, including skin, rubber, stainless steel, and plastics (Fig. 2(c)). Lap shear tests were conducted on the porcine skin and stomach to measure the adhesive strength of HP hydrogels after 5 min of incubation as in the previous work[41] (Fig. 2(d)). The average adhesive strength of the HP hydrogels on the porcine skin decreased from 10.4 to 2.2 kPa as the HTCC/PA ratio decreased from 3 : 1 to 1 : 3 (Fig. 2(e)). The adhesive strength of the HP hydrogel on the stomach varied from 7.7 to 3.7 kPa, which is comparable or slightly higher than that of Celox (Fig. 2(f)). The HP hydrogels with an HTCC/PA ratio of 3 : 1 showed the best adhesive performance. On the porcine stomach surfaces at different pH values, the average adhesive strength of the HP hydrogels was distributed from 3.6 to 0.8 kPa (pH 1), 3.8 to 0.7 kPa (pH 7) and 4.2 to 0.7 kPa (pH 13) (Fig. S1, ESI†). This indicates that the HP hydrogels have a certain adhesive capability on tissue surface, allowing it to perform as a sealing material. The rheological behaviour of the hydrogel was tested by using a rotational rheometer at a fixed frequency of 1 Hz. The gel–sol transition point of HP hydrogels gradually increased with the HTCC/PA ratio increasing from 1 : 3 to 3 : 1, and it slightly decreased from 12.1 kPa to 9.5 kPa when the ratio further increased from 3 : 1 to 6 : 1 (Fig. S2a and b, ESI†). The initial storage modulus (G') and loss modulus (G'') of the HP hydrogels also showed a similar trend (Fig. S2a and c, ESI†). This shows that the strength of HP hydrogels increases with the HTCC/PA ratio increase from 1 : 3

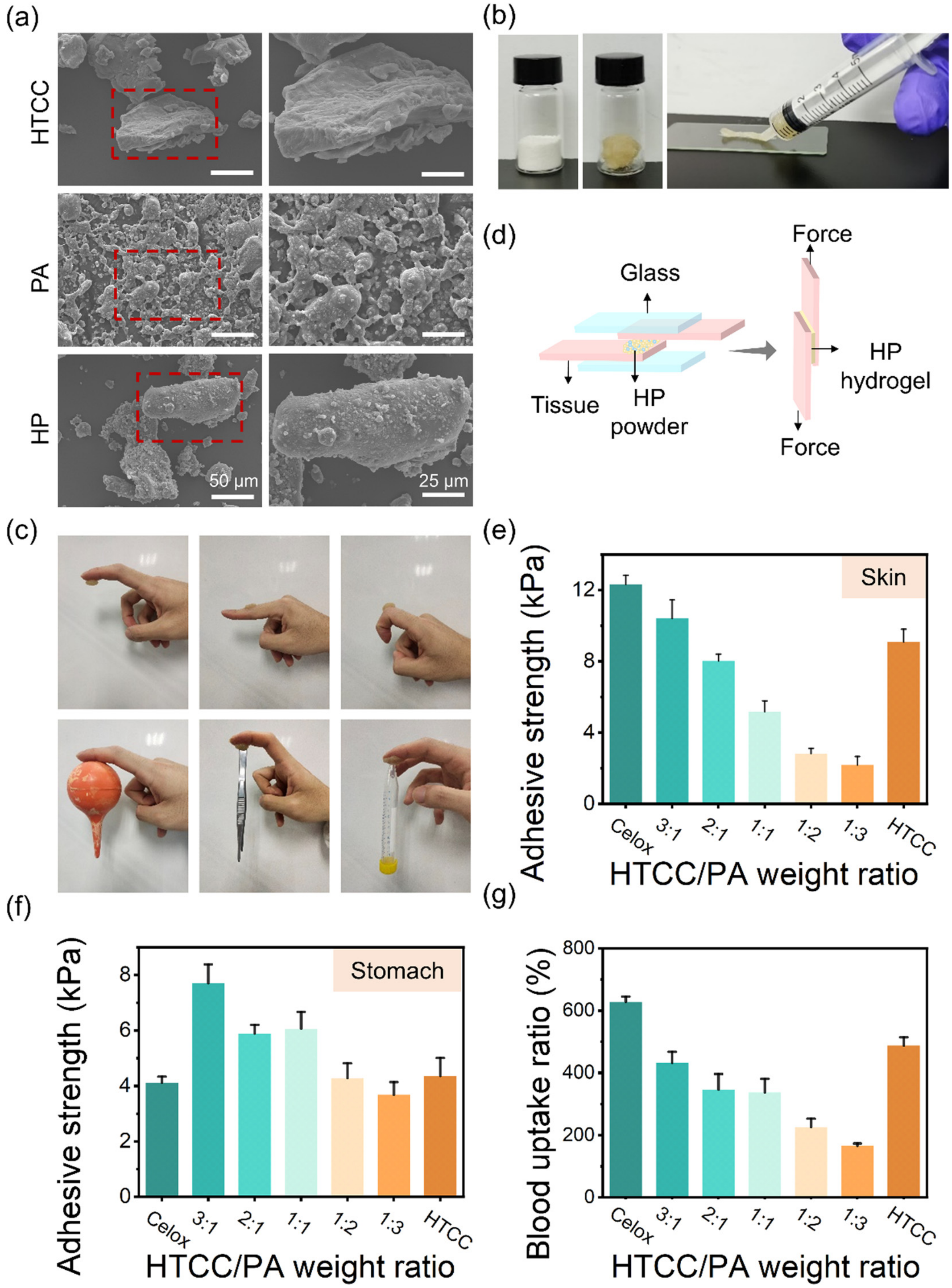

Fig. 2 Characterization of HP hydrogels. (a) SEM images of HTCC, PA, and HP powders. Scale bars represent 50 and 25 μm, respectively. (b) Injectability of HP hydrogel. (c) Universal adhesion of HP hydrogel on versatile surfaces (skin, rubber, stainless steel, and plastics). (d) Schematic illustration of lap shear test, and adhesive strength of hemostatic powders on (e) porcine skins and (f) stomachs. (g) Blood uptake ratio of different hemostatic powders.

to 3 : 1, probably due to the quaternary ammonium groups of HTCC interacting with the phosphate ions of PA, and a further increase in the content of HTCC leads to excessive quaternary ammonium groups in the hydrogel. However, since the HTCC polymer chains could entangle with each other, it still shows a relatively high modulus. In addition, *in vitro* blood absorption tests were conducted by measuring the blood uptake ratio of HP powders.[42] The HP at HTCC/PA ratios of 3 : 1 to 1 : 1 groups all absorbed rat blood up 4.3–3.4 times their self-weight due to the formation of the crosslinked networks (Fig. 2(g)). However, with an increase in PA content, the blood uptake ratio dropped to around 1.6 times their self-weight for an HTCC/PA ratio of

1 : 3. This may be due to the reduced amount of HTCC as well as a looser ionic crosslinking network.

To investigate the performance of the hemostatic powders in the physiological environment of the UGIB, the *in vitro* sealing capacity and acid resistance of the *in situ*-formed HP hydrogels were further evaluated. Firstly, a glass container was fabricated and glued using HP hydrogel, and it was filled with water and placed at room temperature for up to 10 days. As can be seen, no water leakage was observed, although the water level decreased due to evaporation over this period (Fig. 3(a)). In addition, HP hydrogels showed good sealing ability and durability on tissue (pigskin as a demonstration) under an extremely acidic condition (HCl solution at pH 1) for up to 10 days (Fig. S3, ESI†). The resistance of HP hydrogels under neutral conditions and extremely acidic and alkaline conditions was further investigated (Fig. 3(b) and Fig. S4, S5, ESI†), and the mass remaining of the HP hydrogels was monitored (Fig. 3(c)–(e)). At pH 1 (comparable to that in the stomach), HP hydrogels with an HTCC/PA ratio of 3 : 1 to 2 : 1 became white and degraded on Day 3 (Fig. 3(b)) and 35.3% and 46.4% of the mass remained over 10 days, respectively (Fig. 3(c)). No obvious shape changes of the HP hydrogels with an HTCC/PA ratio of 1 : 1 to 1 : 3 was observed (Fig. 3(b)). However, HP hydrogels with an HTCC/PA ratio of 1 : 2 to 1 : 3 showed a higher degradation rate (50.6% and 43.6% remaining, respectively) than the HP hydrogels with an HTCC/PA ratio of 1 : 1 (69.8% remaining) over 10 days, probably due to

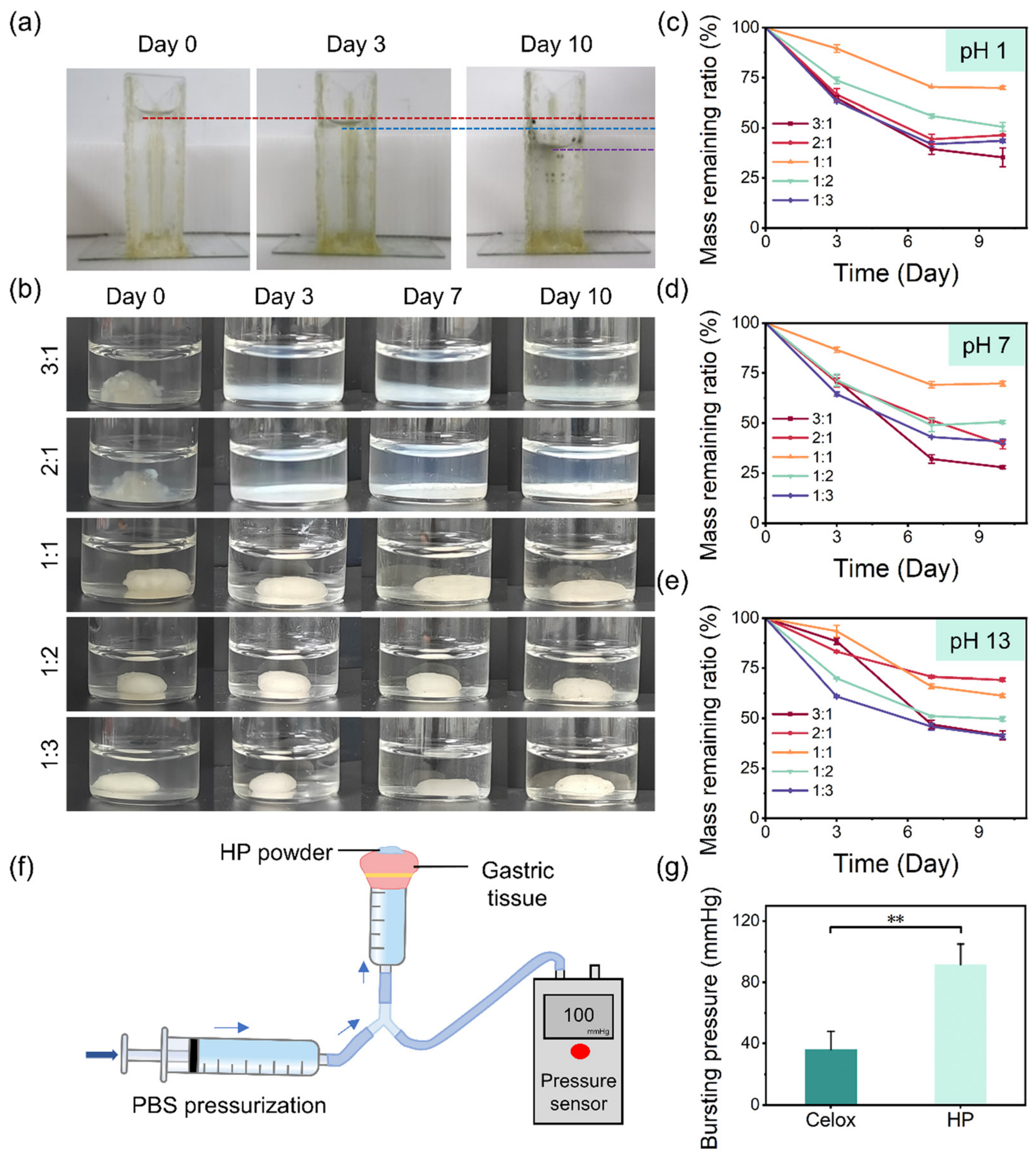

Fig. 3 *In vitro* sealing and acid resistance of HP hydrogel. (a) Sealing performance of HP hydrogels by glueing glass slides to form a container without leakage of water for up to 10 days. (b) Stability of HP hydrogels with various HTCC/PA ratios in HCl solution (pH 1) for up to 10 days. Mass remaining of HP hydrogels at various ratios after incubating in (c) HCl solution (pH 1), (d) deionized water (pH 7), and (e) in NaOH solution (pH 13) for up to 10 days. (f) Schematic illustration of the setup used in the burst pressure test, and (g) bursting pressure of Celox and HP powders on porcine gastric tissue. $^{**}p < 0.01$.

the dissolving of excess PA molecules. The high acid resistance of the HP hydrogel with an HTCC/PA ratio of 1 : 1 can be explained by the excellent deprotonation ability of PA molecules in which six protons are dissociated even in strongly acidic environments,[30,31] facilitating the strong ionic interaction between the positively charged quaternary ammonium groups of HTCC and the negatively charged phosphate groups of PA. This HP hydrogel exhibited a similar tendency in a neutral environment (pH 7) over 10 days (Fig. 3(d) and Fig. S4, ESI†), indicating that HP hydrogels with an HTCC/PA ratio of 1 : 1 had the best stability in neutral and extremely acidic environments. However, the HP hydrogel at a 1 : 1 ratio was not resistant to the highly alkaline condition, as it degraded relatively faster in the solution with a pH of 13 (61.3% remaining over 10 days, Fig. 3(e) and Fig. S5, ESI†), probably due to the low solubility of PA in a high sodium concentration[43] and reduced ionic interactions between HTCC and PA, resulting from the counter ion effect between hydroxide ions in NaOH solutions and quaternary ammonium groups of HTCC.[44] Considering the performance of mechanical properties, stability in acidic environments, and blood absorption capability, we selected the HP formula with an HTCC/PA ratio of 1 : 1 in the rest of this study. The burst pressure of the HP hydrogels sealed on gastric tissue was measured to be 91.6 mmHg, which was higher than that of Celox (36.1 mmHg) and hydrogels used in UGIB previously reported[45] (Fig. 3(f), (g) and Movies S2, S3, ESI†). Thus, it could be anticipated that HP could effectively seal the gastric perforation. These results confirm that the HP hydrogel has a good sealing capability and long-term stability under acidic conditions, which are promising for UGIB applications.

2.2 *In vitro* hemostatic performance

The *in vitro* blood clotting performance of Celox, HTCC, and HP powders was investigated by observing the clotting time of rat whole blood in 96-well plates (Fig. 4(a)). The commercial powder, Celox, established complete clotting within 1 min. In contrast, HTCC dramatically reduced the clotting formation time to 1 min due to the promoted blood cell adhesion by the positively charged quaternary ammonium groups.[21–23] The HP powders developed in this study further shortened the complete progress of clot formation within 15 seconds. Apart from the help of the HTCC, the HP powder could absorb liquids to concentrate the coagulation factors in the blood to generate stable clotting in a short time. Moreover, platelet poor plasma (PPP) was used to investigate the effect of HP powder in the activation of the fibrin formation without platelets as in previous work.[46] The HP powders, as well as HTCC powders, had about 10 seconds of plasma recalcification time (PRT) in the platelet poor plasma, whereas the Celox groups had more than 60 seconds of PRT (Fig. 4(b)). In contrast, quaternary ammonium groups in HTCC promoted the formation of fibrin threads, because of the enhancement of fibrinogen adsorption.[47] To further reveal the mechanisms of the fast hemostasis, adhesion and activation of platelets on the hemostatic powders were investigated using SEM. For HP powders, the activated platelets were observed in the hydrogel networks (Fig. 4(c)). In comparison, platelets merely adhered on the surfaces of Celox powders. In sum, multiple hemostatic mechanisms, including liquid absorption to concentrate coagulation factors, activation and adhesion of platelets, provided the HP powders with outstanding *in vitro* hemostatic performance (Fig. 4(d)).

2.3 *In vivo* hemostatic capability and on-demand removable properties

To further investigate the *in vivo* hemostatic performance of HP powders, rats with a tail bleeding model and liver injury model were used (Fig. 5). The blood loss and bleeding time for hemostasis were recorded. In the rat tail bleeding model, the rat tail was excised ∼10 cm from its base under anaesthesia (Fig. 5(a) and Movies S4–S6, ESI†). Compared with the average blood loss (2960.0 mg) and bleeding time (>600 seconds) of the blank group, Celox reduced the blood loss and bleeding time to 1933.3 mg and 310.3 seconds, respectively (Fig. 5(b) and (c)). HP powders further decreased the blood loss and hemostasis time to 1006.7 mg and 208.3 seconds, respectively. In the liver injury model, the rat liver was cut with a length of ∼2 cm under anaesthesia (Fig. 5(d) and Movies S7–S9, ESI†). The average blood loss decreased significantly from the blank group (1433.3 mg) to 736.7 mg for the Celox group and 263.3 mg for the HP group (Fig. 5(e)). Besides, the average bleeding time also dropped dramatically from 291.3 seconds (blank group) to 183.7 seconds (Celox powder) and 142.0 seconds (HP powder) (Fig. 5(f)). Furthermore, HP powders showed stable adhesion on rat tail bleeding (Movies S4–S6, ESI†) and liver injuries (Movies S7–S9, ESI†). HP hydrogels on the wounds of the tails or liver were hardly flushed away by physiological saline solution (Fig. S6 and Movies S6, S9, ESI†). The HP hydrogels showed no blood leakage from the wound after scraping by forceps, while the Celox powders showed substantial leakage after scraping by forceps (Fig. S6 and Movies S5, S8, ESI†). The stable sealing capability of the HP hydrogel is probably due to the stable clots formed from the crosslinking with HP networks, activated platelets, and fibrins on wounds. This is extremely important as rebleeding is a serious issue in UGIB. Interestingly, the formed HP hydrogels on the rat gastric perforation site could be removed easily and selectively by rinsing with sodium bicarbonate solution after the bleeding was successfully stopped (Fig. S7 and Movie S10, ESI†). This may be because of the ion shielding effect due to the ions in sodium bicarbonate solutions forming a charge barrier to damage the electrostatic interactions and hydrogen bonding between the HP hydrogel and tissue surface to decrease the adhesion dramatically and rapidly. In addition, the high ionic strength of sodium bicarbonate solution could also reduce the solubility of PA molecules[43] and decrease the adhesion of the hydrogel. This on-demand removability of HP hydrogels would prevent excessive adhesion to other internal surfaces. Therefore, the HP powders exhibited excellent *in vivo* hemostatic and sealing performance and selectively removable behaviours simultaneously, which are all important properties for the treatment of UGIB.

2.4 *In vitro* biocompatibility and *in vivo* liver healing

The hemocompatibility, cytotoxicity, and healing effect of liver tissues after injury were conducted to investigate the

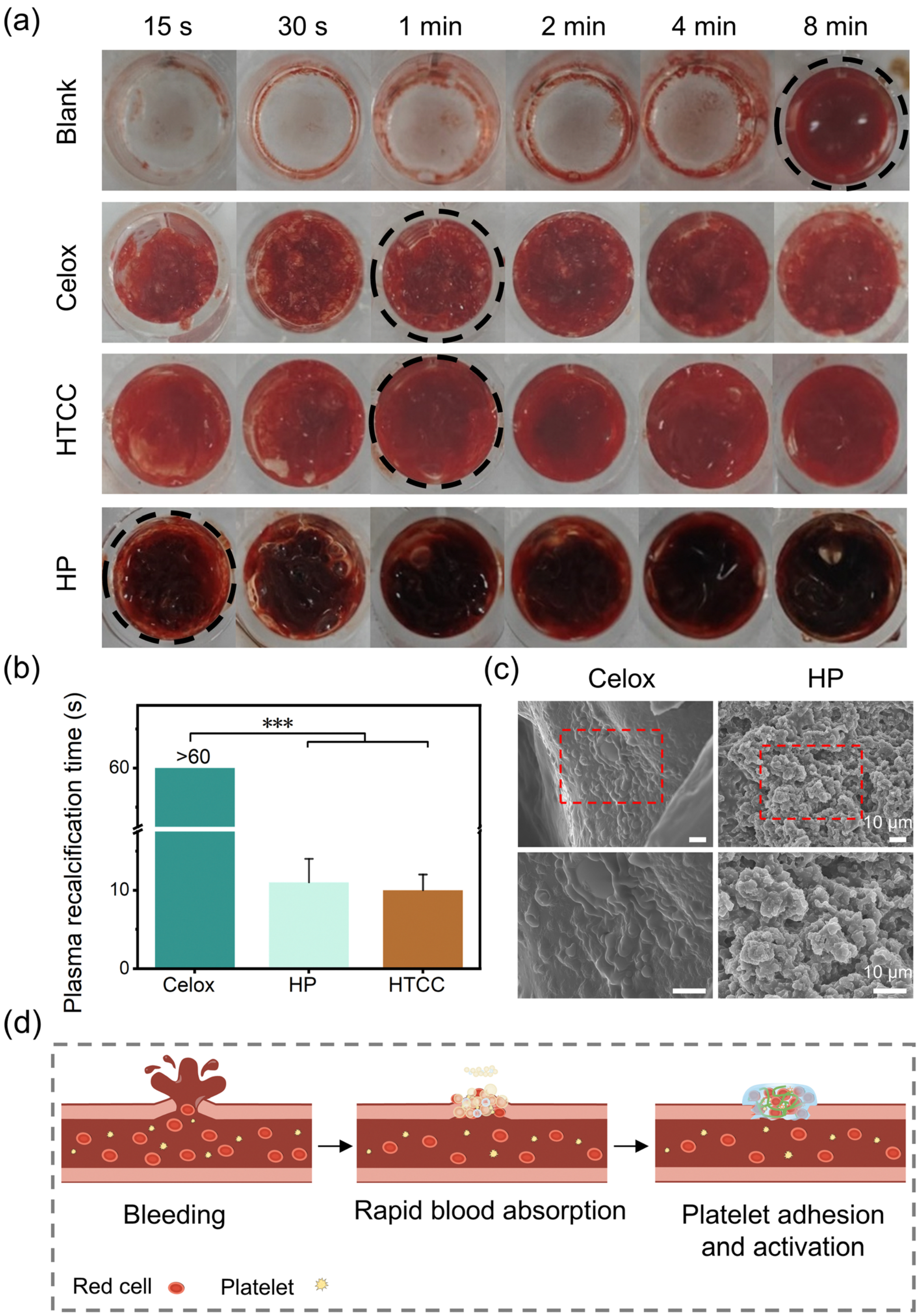

Fig. 4 *In vitro* blood clotting performance of hemostatic powders. (a) Digital photographs of the clotting time of rat whole blood with the addition of hemostatic powders. (b) PRT of hemostatic powders. (c) SEM images of platelet adhesion on Celox and HP powders. Scale bar: 10 μm. (d) Schematic illustration of the possible hemostatic mechanisms of HP powders. ***$p < 0.001$.

biocompatibility of HP hydrogels. In the hemolysis test, 5% erythrocyte saline solution was used to incubate Celox and HP powders at 37 °C for 30 min. After centrifugation, the absorbance of the supernatant at 540 nm was recorded to determine the hemolysis ratios (Fig. 6(a)). The hemolysis ratios of Celox and HP powders were all below 5%, which is in the safe range for hemostatic materials. Moreover, rat fibroblasts (RS1) were used to test the *in vitro* cytotoxicity of the hemostatic powders. The viability of cells incubated in extracts of Celox powder and HP powder for 24 h was over 95% and showed no significant difference compared with the negative control (the sesame oil/DMEM mixture) (Fig. 6(b)). The good cell compatibility can be explained by the ion shielding effect between phosphate groups of PA with quaternary ammonium groups of HTCC. Therefore, a great advantage of assembling HTCC and PA to create HP powders and hydrogels is the mitigation of the

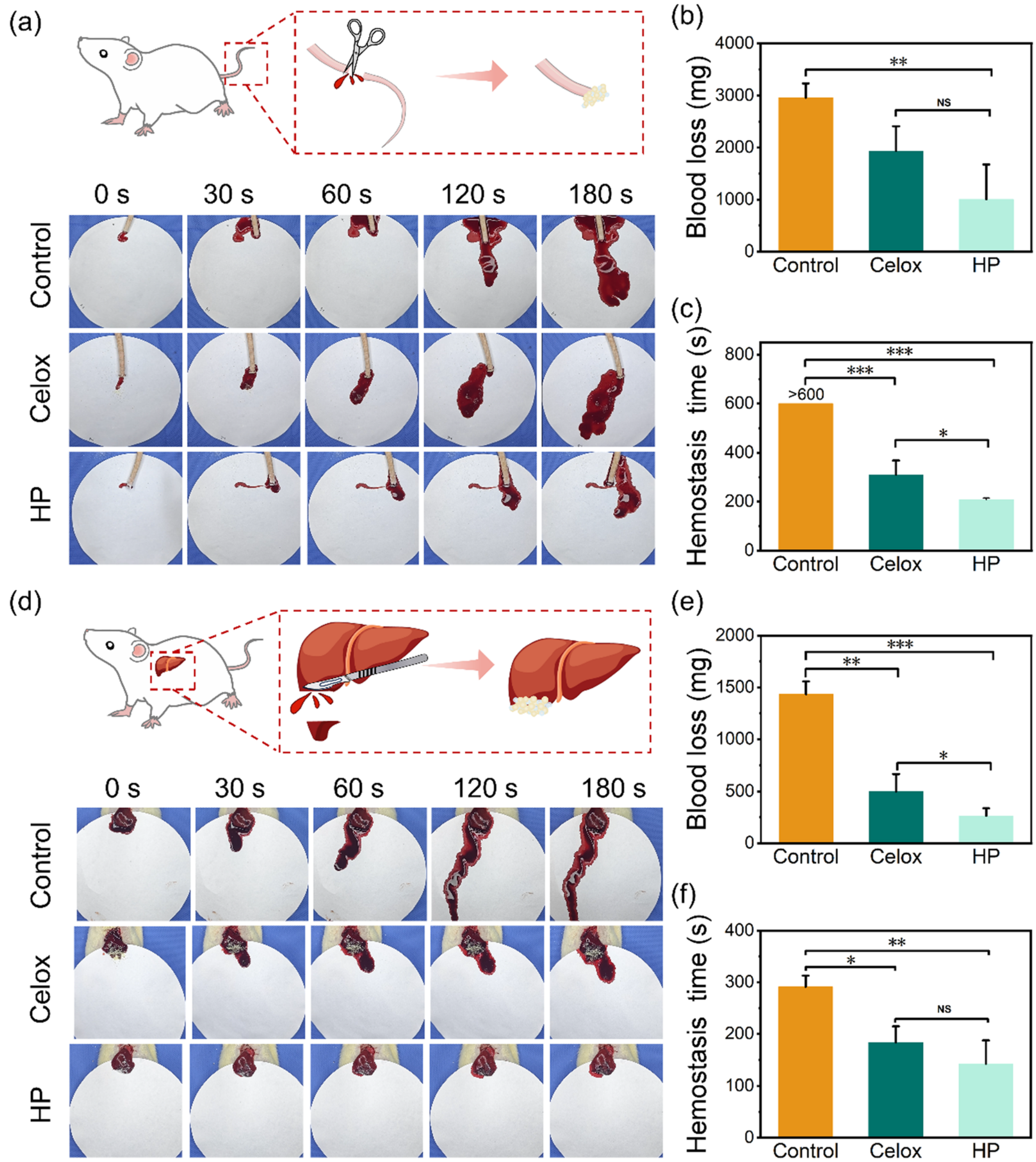

Fig. 5 *In vivo* hemostatic capability in a rat model. (a) Schematic illustration of the rat tail bleeding model and photographs of tail hemostasis in the different groups. Quantitative analysis of (b) blood loss and (c) hemostasis time in the tail bleeding model. (d) Schematic illustration of the rat liver injury model and photographs of liver hemostasis in the different groups. Quantitative analysis of (e) blood loss and (f) hemostasis time in the liver injury model. $*p < 0.05$, $**p < 0.01$ and $***p < 0.001$, NS denotes no significance.

cytotoxicity of HTCC, thereby expanding its application in biomedical fields.

The healing performance of the liver that was injured and treated with hemostatic powders in the liver injury experiment (Fig. 5(b)) was evaluated after the animals were fed normally for 14 days (Fig. 6(c)). From the images of hematoxylin–eosin (H&E) staining, the control group (the wound was left without treatment) showed large and uniform coverage of red blood cells in blood vessels and liver hepatocytes, which indicated a high inflammatory level due to the liver injury. The Celox group had a small amount of blood oozing in the liver and aggregated red blood cells in the vessels. In contrast, the HP showed some anti-inflammatory performance since only a few erythrocytes were present in the blood vessels. This was likely due to the high blood uptake of the HP powders after the bleeding and the good anti-inflammatory properties of PA.[34–36] Furthermore, the expression of cell adhesion molecule 31 (CD31) and cytokeratin 19 (CK19) was assessed to evaluate the regeneration of blood vessels and bile ducts in the liver tissue, which are crucial in liver regeneration because of their roles in oxygen supply and nutrition transportation,[48–50] and hepatocyte transdifferentiation.[48,51] Compared with the sham group and Celox group, the HP group exhibited better performance in liver regeneration. More endothelial cells (CD31+) and cholangiocytes (CK19+) were differentiated and present in the HP group, indicating better reconstruction of the blood vessels and bile duct systems, respectively. Chitosan-based materials have been shown to promote neovascularization and cell proliferation.[18–20]

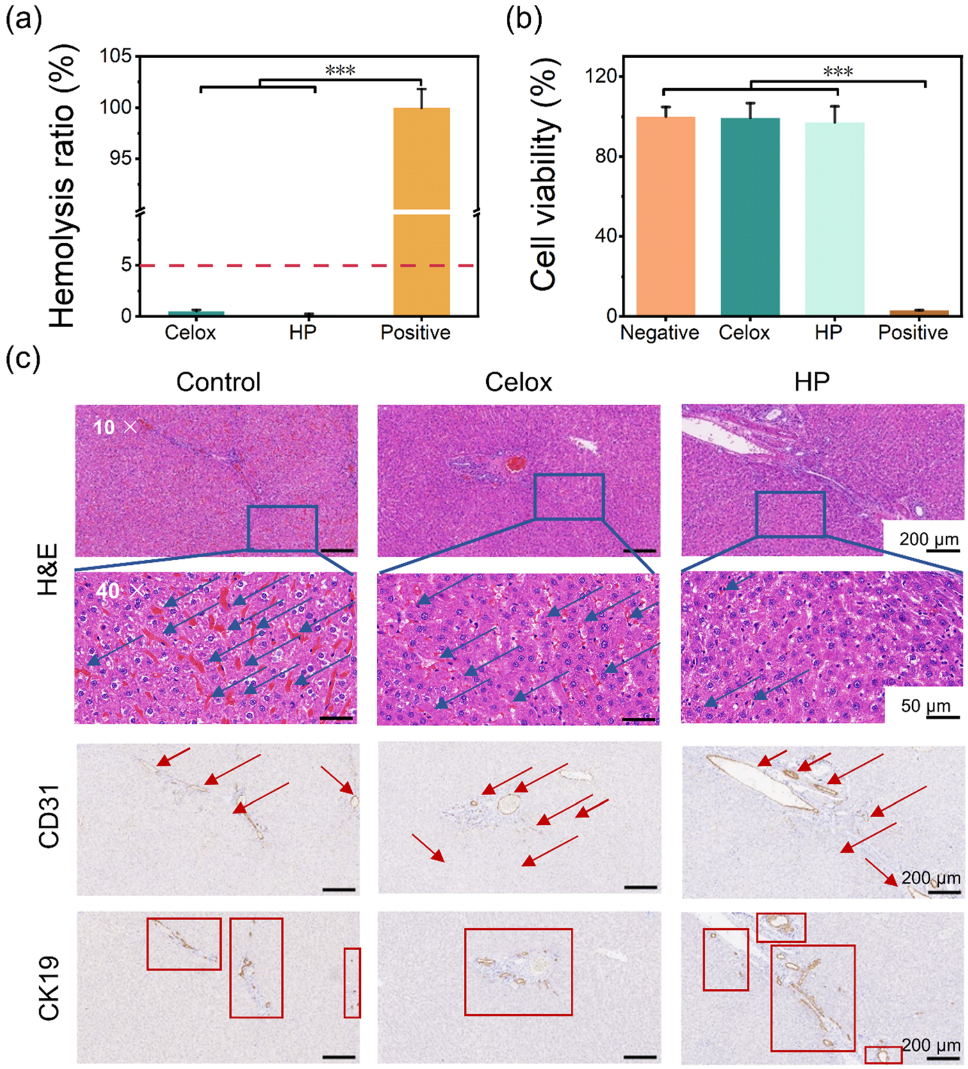

Fig. 6 *In vitro* and *in vivo* biocompatibility. (a) Hemocompatibility of hemostatic powders. Positive control: 0.1% Triton-X. (b) Cell viability of RS1 cells after incubation with leachate of hemostatic powders for 24 h. Negative control: sesame oil/DMEM mixture. Positive control: 10 mg mL^{-1} zinc diethyldithiocarbamate medium. (c) H&E, CD31 (indicating endothelial cells), and CK19 (indicating cholangiocytes) staining images of liver tissues after the animals were subjected to a liver injury experiment and fed for 14 days. Blue arrows: erythrocytes. Red arrows: blood vessels. Red rectangle: bile ducts. $^{***}p < 0.001$.

In sum, HP powders have good *in vitro* and *in vivo* biocompatibility and capability for promoting tissue healing.

2.5 *In vivo* sealing capability of gastric perforation

The *in vivo* sealing performance of HP powder was investigated by using a rat gastric perforation model (Fig. 7(a)). After fasting for 24 h, Sprague-Dawley rats were anaesthetized, and the stomach was perforated by using a scalpel. Two milligrams of HP powder were added to the wound site to seal the perforation. Glucose and antibiotics were fed to the rats during the initial three days. After 14 days, the gastric tissues were collected to observe the sealing performance and were stained by H&E staining to evaluate wound healing. The perforation site was closed by the sutures in the sham control group. By comparison, the *in situ*-formed HP hydrogel (mixed with gastric contents, indicated by the yellow arrow) sealed the incision part firmly and resisted in the acidic environment in the stomach for two weeks (Fig. 7(b)). In histological staining (Fig. 7(c)), the sham group had irregular and incomplete gastric mucosa and aggregated red blood cells beneath the mucosa, indicating an inflammatory reaction and unhealed gastric tissues. However, the HP group exhibited promoted tissue regeneration in the stomach which had neovascularization and regular and thick mucosa comparable with the normal gastric tissues (blank group). This showed that HP powders had good *in vivo* gastric sealing capability over a prolonged period, and it could promote the healing of gastric wounds effectively.

3. Conclusion

In this work, HTCC/PA (HP) powders representing promising advancements in hemostatic materials for managing UGIB

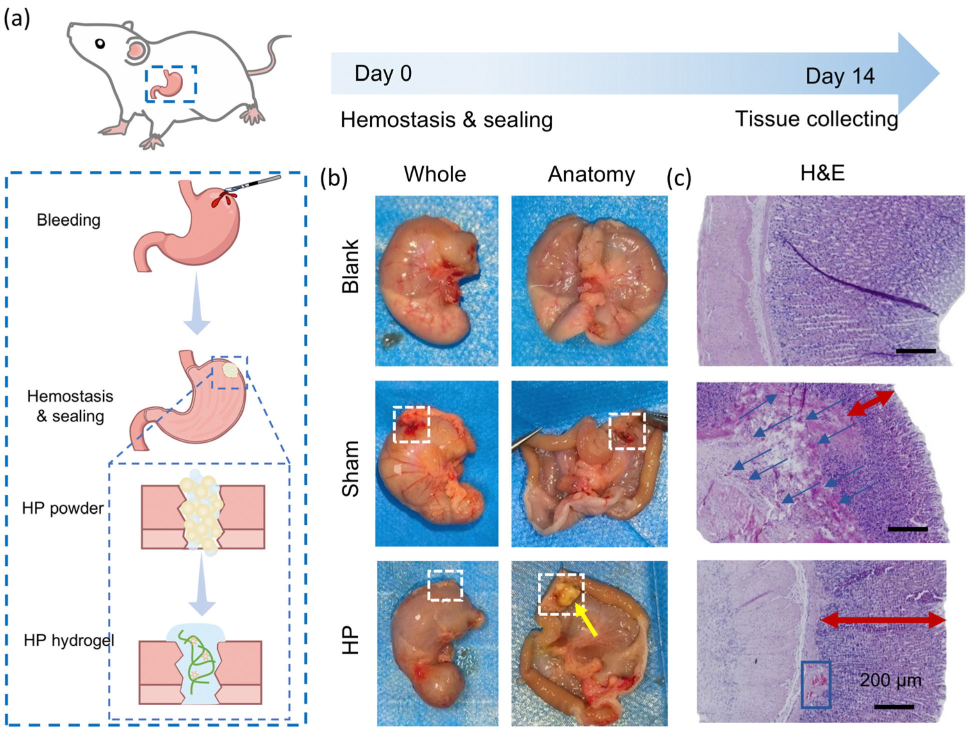

Fig. 7 *In vivo* gastric sealing performance. (a) Schematic illustration of HP powders' gelation and sealing on the rat's gastric perforation site. (b) Photographs of gastric wounds treated with sham operation and HP powders after 14 days. White rectangle: wound site. Yellow arrow: remaining HP hydrogel. (c) H&E staining of the tissues at the gastric perforation sites after 14 days. Red arrows: thickness of healed mucosa. Blue arrows: red blood cells. Blue rectangle: blood vessels. Scale bar: 200 μm.

have been developed utilizing the strong electrostatic interactions between HTCC and PA. The hydrogels exhibit rapid gelation, exceptional acid resistance, and appropriate adhesive properties in both *in vitro* and simulated *in vivo* environments. Their ability to quickly halt bleeding, promote clotting, and maintain stability under acidic conditions *in vitro* and *in vivo* highlights their potential for clinical application. Impressively, HP powders can be easily removed by using salt solutions. This offers additional clinical flexibility, ensuring ease of application and removal as needed. Furthermore, the biocompatibility assessments have confirmed minimal cytotoxicity and favourable tissue regeneration, thereby supporting their safety and efficacy. HP powders at micron sizes are expected to be delivered to the operational site in the stomach by using compressed air through a catheter, ensuring their applicability in the clinic. Overall, HP powders present a novel strategy for improving UGIB management which warrants further investigation and clinical validation.

4. Experimental section

4.1 Materials

N-[(2-Hydroxy-3-trimethylammonium) propyl] chitosan chloride (HTCC, 95%) was purchased from Macklin (Shanghai, China). Phytic acid (PA, 98%) was purchased from Energy Chemical (Anhui, China). Commercial hemostatic powder (Celox) was purchased from Medtrade Products (United Kingdom). All chemicals are of analytical grade and ready to use.

4.2 HP powder and hydrogel preparation

HTCC and PA were weighed in the ratios of 3 : 1 to 1 : 3 with a total weight fixed at 100 mg and vortexed for 1 min for mixing. One hundred microlitres of deionized water or whole blood was added to 100 mg HTCC/PA powder to obtain HP hydrogel.

4.3 Material characterization

HTCC, PA, and HP powders were characterized using Fourier transform infrared (FT-IR) spectroscopy (Nicolet-iS50, Thermo-Fisher) in the wavenumber range of 500–4000 cm^{-1}. The morphology of the HP powders was observed using a SEM (S4800, Hitachi).

4.4 Gelation time and injectable behaviour

Gelation time was determined by inverting a sample bottle containing 200 mg of HP powder mixed with 200 μL deionized water until no flow was observed. Injectable behaviour was assessed by observing the HP hydrogel from syringe extrusion.

4.5 Tissue adhesive tests

Tissue adhesion strength of HP hydrogels was evaluated *via* the lap shear test using a Universal Testing Machine (CMT-1104, SUST, China). Fresh pig skin and stomach were obtained from a local market, cleaned to remove the oily substances, and cut into strips (75 mm × 25 mm). One hundred milligrams of HP powders were applied to an area 20 mm × 20 mm from the end of one tissue strip, and another tissue strip overlapped with it. The HP powders would absorb the excess moisture on the tissue to transit to hydrogels. Then, the setup was fixed with two glass slides and held with a clamp for 5 min. The assembly was pulled using the Universal Testing Machine at a rate of 50 mm s^{-1} and the force–displacement curves were recorded. To evaluate the adhesion strength on tissues with different pH values, pig stomach strips were immersed in deionized water (pH 7), HCl solution (pH 1), or NaOH solution (pH 13) for 5 min. The tissues were then used in the adhesion test as described above.

4.6 Rheological properties

Rheological testing of HP hydrogels was conducted using a rotational rheometer (WATERS, HR-2) by adding 200 μL of deionized water to 200 mg HP powders with different HTCC/PA ratios on a test plate, and measuring the rheological behaviour at a fixed frequency of 1 Hz.

4.7 Blood absorption capability

Two hundred microlitres of anticoagulated rat whole blood were added into 10 mg of Celox, HTCC powder, or HP powder with different HTCC/PA ratios. After gentle shaking for 30 seconds, the remaining blood was quickly aspirated, and the absorbed weight was recorded. The blood uptake ratio was calculated as follows:

$$\text{Blood uptake ratio (\%)} = (w_t - w_0)/w_0 \times 100\%$$

where w_0 is the initial weight of the powder, and w_t is the weight after the powder takes up blood.

4.8 *In vitro* sealing performance

Four glass slides were glued to form a container of triangular prism by using the formed HP hydrogels. The glass container was filled with deionized water and the watermark was recorded on days 0, 3, and 10. In addition, an incision (5 mm × 1 mm) was created in a pig skin (4 cm × 4 cm) that was soaked with an antimicrobial agent solution (0.5% heptyl 4-hydroxybenzoate solution), and HP powder was used to block the incision. A cylindrical quartz container (diameter: 13 mm) was fixed to the pig skin using superglue, and 1 mL of HCl solution (pH 1) was added. The setup was placed in a Petri dish containing an antimicrobial solution with a water level similar to the thickness of the pig skin to avoid drying and rotting of the tissue. The setup was recorded by photography on days 0, 3, 7, and 10.

4.9 *In vitro* stability test

One hundred milligrams of HP hydrogels were immersed in 2 mL of deionized water (pH 7), HCl (pH 1) or NaOH solution (pH 13). Photos were taken on days 0, 3, 7, and 10 to evaluate the resistance of the hydrogels to acidic and alkaline environments. In addition, the remaining hydrogels on days 0, 3, 7, and 10 were freeze-dried and weighted. The mass remaining ratio was calculated as below:

$$\text{Mass remaining ratio (\%)} = m_t/m_0 \times 100\%$$

where m_0 is the initial mass of the powder, and m_t is the mass of the freeze-dried powder after degradation.

4.10 Burst pressure test

A circular piece of porcine gastric tissue (8 cm in diameter) was fixed onto the end of the syringe barrel using a rubber band. A 2 mm diameter notch was made to the gastric tissue by needle penetration. The setup was connected to another syringe filled with phosphate-buffered saline (PBS, 10 mM) and a pressure sensor *via* a tee junction and silicone tubes. PBS was injected *via* a syringe pump. The syringe was pushed to fill the device with PBS. The notch in the gastric tissue was then sealed with 200 mg of powders (Celox or HP). After 2 min for stabilization, PBS was injected *via* the syringe pump at a rate of 120 L h^{-1} to inflate the gastric tissue. The maximum pressure before the failure of the sealing was considered as the burst pressure.

4.11 Blood clotting time tests

Fifty milligrams of Celox, HTCC, and HP powders were placed into the well of a 96-well plate. One hundred microlitres of rat whole blood mixed with 0.1 M of $CaCl_2$ at a ratio of 9 : 1 was added to the well. The unclotted portions were removed by rapidly adding an appropriate amount of PBS (10 mM, pH 7.4) at predetermined time points. The clotting time was recorded when uniform clots appeared.

4.12 *In vitro* platelets adhesion

Ten millilitres of anticoagulated rat whole blood was centrifuged at 2500 rpm for 10 min to obtain platelet-rich plasma (PRP) in the middle layer. Fifty milligrams of Celox and HP powders were added to a 6-well plate, to which 100 μL of PRP was dropped and incubated for 30 min at 37 °C. All samples were washed three times with PBS to remove unattached platelets, and fixed overnight with 2.5 wt% glutaraldehyde. Gradual dehydration was performed using ethanol solutions (50%, 60%, 70%, 80%, 90%, and 100%) at 10 min intervals. After drying at 37 °C for 12 h, the samples were observed by SEM.

4.13 *In vitro* plasma recalcification time (PRT)

Anticoagulated rat whole blood was centrifuged at 3000 rpm for 20 min to obtain the platelet poor plasma (PPP), 50 μL of which was preheated to 37 °C for 10 min and added onto the glass surface (preheated to 37 °C). Ten milligrams of powder samples and 10 μL of $CaCl_2$ solution (0.025 M, preheated to 37 °C) were added to PPP immediately. A stainless steel hook was used to dip in the solution to observe the appearance of fibrin threads. The duration between the addition of $CaCl_2$ solutions and the formation of continuous fibrins was recorded as the plasma recalcification time (PRT).

4.14 *In vivo* hemostatic properties

All animal experiments were performed in compliance with the laboratory animal-guidelines for ethical review of animal welfare (GB/T35892-2018), and approved by the Institutional Animal Care and Use Committee of Ningbo Institute of Life and Health Industry (approval number: GK-2024-LW-0017). Sprague-Dawley rats (SD rats, male, 6–8 weeks, 250–300 g, purchased from Zhejiang Vital River Laboratory Animal Technology) were randomly divided into the blank group, Celox group, and HP group. The hemostatic effect of powders was evaluated by the rat tail bleeding model and rat liver injury model. In the rat tail bleeding model, rats were anesthetized with 2% sodium pentobarbital, and filter paper was placed under the tail. A cut was made 10 cm away from the tail base with surgical scissors, and 200 mg of hemostatic powders was immediately sprinkled on the bleeding site, which was pressed gently. The bleeding time and blood loss were recorded for each group. After 5 min, the wound was rinsed with 0.9% saline or scraped off with forceps and the sealing effect of the wound by the powders was observed. In the rat liver injury model, rats were anesthetized as described above, and the abdomen was dissected with the liver exposed. Filter paper was placed under the liver and a 2 cm length of tissue was excised from the lower part of the liver using a scalpel. Two hundred milligrams of hemostatic powders were quickly sprinkled on the bleeding site, which was pressed gently. The bleeding time and blood loss were recorded as described above. Meanwhile, after 5 min, the wound was rinsed with 0.9% saline or scraped off with forceps to observe the sealing effect of the hemostatic powder on the wound.

4.15 Cytotoxicity assay

Powder samples were subjected to a leachate test to assess their cytotoxicity. Since the high solubility in water, Celox, and HP powders were immersed in sesame oil (200 mg mL^{-1}) at 37 °C for 72 h. Rat fibroblasts (RS1) were seeded in 96-well plates (1×10^4 cells per well) and cultured in Dulbecco's Modified Eagle's Medium (DMEM, Gibco, United States) supplemented with 10% fetal bovine serum (FBS, Gibco, United States) and 1% antibiotics (penicillin and streptomycin) for 24 h at 37 °C in a humidified 5% CO_2 incubator. The medium was replaced with each powder extract and DMEM at a volume ratio of 1 : 9. Sesame oil/DMEM mixture and 10 mg mL^{-1} zinc diethyldithiocarbamate medium served as the negative and positive controls. After 24 h of incubation, cell viability was assessed using the cell counting kit-8 (CCK-8, TransGen Biotech, China) according to the manufacturer's instructions.

4.16 Hemolysis assay

Three millilitres of rat anticoagulated blood was centrifuged at 2500 rpm for 10 min, and the erythrocyte layer was collected after removing the supernatant. The collected erythrocytes were washed with PBS three times and suspended in 0.9% saline to create a 5% erythrocyte saline solution. Fifty milligrams of powders (Celox and HP) were immersed in 1 mL of 0.9% saline at 37 °C for 24 h to obtain sample eluates. One hundred microlitres of each sample eluate was mixed with 900 μL of erythrocyte suspension. Physiological saline solution and 0.1% Triton-X were used as the negative and positive controls. Samples were incubated at 37 °C for 30 min, followed by centrifugation at 2500 rpm for 5 min. The absorbance of the supernatant at 540 nm was measured using a microplate reader. The hemolysis ratio was calculated using the formula:

$$\text{Hemolysis ratio (\%)} = (OD_S - OD_N)/(OD_P - OD_N) \times 100\%$$

where OD_S is the absorbance value of the sample, OD_N is the absorbance value of the negative control, and OD_P is the absorbance value of the positive control.

4.17 Tissue compatibility test and *in vivo* liver wound healing effects

To evaluate biocompatibility and tissue regeneration, histological analysis was performed using a hepatic defect hemorrhage model. After hemostasis of the liver defect site as described above, the rat abdomens were sutured, and the animals were fed normally. After 14 days, the animals were sacrificed and the livers were collected, fixed in 4% paraformaldehyde, dehydrated, and embedded in paraffin. The expression of cell adhesion molecule 31 (CD31, Abcam ab281583) and cytokeratin 19 (CK19, Abcam ab52625) was quantified using immunohistochemistry staining to observe blood vessel and bile duct growth. Histological analysis of the liver tissues was conducted after H&E staining.

4.18 *In vivo* gastric perforation sealing

After fasting for 24 h, SD rats were anaesthetized, and a midline abdominal incision was made to expose their stomachs. A 0.5 cm vertical perforation was created at the stomach base using a scalpel. Two hundred milligrams of HP powder was applied quickly onto the wound for hemostasis. A blank group (stomach without perforation) and a sham operation group (stomach with perforation that was sutured) were included for comparison. Glucose and antibiotics were administered to the rats during the initial three days of gastric perforation healing. After 14 days, the rats were euthanised, their abdomens were dissected, their stomachs were exposed, and the wound healing sites were photographed. Stomach tissues were fixed in a 4% paraformaldehyde solution, dehydrated, and embedded in paraffin. The paraffin-embedded samples were cut into 5 μm sections, deparaffinised using xylene, and dehydrated with ethanol gradients, stained, and finally examined under a microscope.

4.19 *In vivo* on-demand removable ability

Rats were anaesthetised using 2% sodium pentobarbital and the abdomen was dissected to expose the stomach. A 1 cm wound was made on the surface of the stomach with a razor blade and 100 mg of HP powder was immediately applied to the wound. After hemostasis ($\sim$2 min), the wound was rinsed with 2 mL of 2.5% sodium bicarbonate solution and the powders were gently wiped away with gauze.

4.20 Statistical analysis

Data are presented as means ± standard deviation ($n \geq 3$). The significance of the results was determined using one-way analysis of variance (ANOVA). The significant levels were denoted as $*p < 0.05$, $**p < 0.01$ and $***p < 0.001$.

Author contributions

Ashuang Liu: conceptualization, investigation, methodology, data curation, writing – original draft. Zhimao Huang: conceptualization, investigation, methodology, data curation, writing – original draft. Shengyong Cui: data curation, methodology. Ying Xiao: methodology. Xiangshu Guo: methodology. Gaoke Pan: methodology. Lei Song: methodology. Junjie Deng: methodology. Ting Xu: methodology. Youfen Fan: methodology, funding acquisition. Rong Wang: supervision, project administration, funding acquisition, conceptualization, writing – review & editing.

Data availability

The data sets used to generate the results in this work are available at **https://dataspace.nimte.ac.cn:8080/space/1524644026781818880/details/filesManage**.

Conflicts of interest

The authors declare no conflicts of interest.

Acknowledgements

This work was supported by the Youth Innovation Promotion Association CAS (2021296), the Key Research and Development Program of Ningbo (2022Z132), Joint Funds of the Zhejiang Provincial Natural Science Foundation of China (LZY24H150001), Zhejiang Provincial Natural Science Foundation of China (LQ21E030006), Ningbo Public Welfare Science and Technology Plan Project (2023S020), the Foundation of Director of Ningbo Institute of Materials Technology and Engineering CAS (2021SZKY0301), the Ningbo Top Medical and Health Research Program (2023030615), the Project of Ningbo Leading Medical & Health Discipline (2022-F17), and Zhejiang Provincial Medical and Health Science and Technology Program Project (2021KY1004).

References

1 B. S. M. Kim, *World J. Gastrointest. Pathophysiol.*, 2014, **5**, 467.
2 J. Orpen-Palmer and A. J. Stanley, *BMJ Med.*, 2022, **1**, e000202.
3 M. E. Van Leerdam, *Best Pract. Res. Clin. Gastroenterol.*, 2008, **22**, 209–224.
4 D. T. De Rezende, V. O. Brunaldi, W. M. Bernardo, I. B. Ribeiro, R. C. L. Mota, F. I. Baracat, D. T. H. De Moura, R. Baracat, S. E. Matuguma and E. G. H. De Moura, *Endosc. Int. Open*, 2019, **07**, E1704–E1713.
5 L. H. S. Lau and J. J. Y. Sung, *Dig. Endosc.*, 2021, **33**, 83–94.
6 B. R. Freedman, O. Uzun, N. M. M. Luna, A. Rock, C. Clifford, E. Stoler, G. Östlund-Sholars, C. Johnson and D. J. Mooney, *Adv. Mater.*, 2021, **33**, 2008553.
7 S. F. Elahi and T. D. Wang, *J. Biophotonics*, 2011, **4**, 471–481.
8 M. Cui, M. Zhang and K. Liu, *Carbohydr. Polym.*, 2021, **272**, 118530.
9 D. Shahsavari and H. P. Parkman, in *Nutrition, Weight, and Digestive Health*, ed. C. Newberry, J. Laster and O. Pickett-Blakely, Springer, Cham, Switzerland, 2022, ch. 1, pp. 3–28.
10 P. T. Ramsay and A. Carr, *Surg. Clin. North Am.*, 2011, **91**, 977–982.
11 L. Krishnan, *Biomaterials*, 2004, **25**, 5557–5563.
12 A. Basu, J. Hong and N. Ferraz, *Macromol. Biosci.*, 2017, **17**, 1700236.
13 K. Jiang, Y.-Z. Long, Z.-J. Chen, S.-L. Liu, Y.-Y. Huang, X. Jiang and Z.-Q. Huang, *Nanoscale*, 2014, **6**, 7792.
14 S. X. Jiang, D. Chahal, N. Ali-Mohamad, C. Kastrup and F. Donnellan, *Endosc. Int. Open*, 2022, **10**, E1136–E1146.
15 D. H. Jung, C. H. Park, S. I. Choi, H. R. Kim, M. Lee, H. S. Moon and J. C. Park, *Clin. Gastroenterol. Hepatol.*, 2023, **21**, 2844–2853.
16 X. Peng, X. Xia, X. Xu, X. Yang, B. Yang, P. Zhao, W. Yuan, P. W. Y. Chiu and L. Bian, *Sci. Adv.*, 2021, **7**, eabe8739.
17 J. Guo, L. Ye, Y. Gao, S. Li, L. Zhang, W. Liu, T. Peng, Y. Mou, C. Wu, C. Xie, B. Hu and X. Deng, *ACS Nano*, 2023, **17**, 9521–9528.
18 A. L. Harkins, S. Duri, L. C. Kloth and C. D. Tran, *J. Biomed. Mater. Res., Part B*, 2014, **102**, 1199–1206.
19 I. Bano, M. Arshad, T. Yasin, M. A. Ghauri and M. Younus, *Int. J. Biol. Macromol.*, 2017, **102**, 380–383.
20 H. Ueno, T. Mori and T. Fujinaga, *Adv. Drug Delivery Rev.*, 2001, **52**, 105–115.
21 X. Zhao, H. Wu, B. Guo, R. Dong, Y. Qiu and P. X. Ma, *Biomaterials*, 2017, **122**, 34–47.
22 H. Gao, Z. Zhong, H. Xia, Q. Hu, Q. Ye, Y. Wang, L. Chen, Y. Du, X. Shi and L. Zhang, *Biomater. Sci.*, 2019, **7**, 2571–2581.
23 X. Zhao, B. Guo, H. Wu, Y. Liang and P. X. Ma, *Nat. Commun.*, 2018, **9**, 2784.
24 L. Wang, X. Zhang, K. Yang, Y. V. Fu, T. Xu, S. Li, D. Zhang, L. Wang and C. Lee, *Adv. Funct. Mater.*, 2020, **30**, 1904156.
25 X. Du, Y. Liu, H. Yan, M. Rafique, S. Li, X. Shan, L. Wu, M. Qiao, D. Kong and L. Wang, *Biomacromolecules*, 2020, **21**, 1243–1253.
26 J. Qu, X. Zhao, Y. Liang, T. Zhang, P. X. Ma and B. Guo, *Biomaterials*, 2018, **183**, 185–199.
27 Z.-X. Peng, L. Wang, L. Du, S.-R. Guo, X.-Q. Wang and T.-T. Tang, *Carbohydr. Polym.*, 2010, **81**, 275–283.
28 K. Pathak, S. K. Misra, A. Sehgal, S. Singh, S. Bungau, A. Najda, R. Gruszecki and T. Behl, *Polymers*, 2021, **13**, 2514.

29 W. Chen and D. Xu, *Trends Food Sci. Technol.*, 2023, **141**, 104201.
30 R. Angel, N. M. Tamim, T. J. Applegate, A. S. Dhandu and L. E. Ellestad, *J. Appl. Poult. Res.*, 2002, **11**, 471–480.
31 R. Wang and S. Guo, *Compr. Rev. Food Sci. Food Saf.*, 2021, **20**, 2081–2105.
32 I. Abdulwaliyu, S. O. Arekemase, J. A. Adudu, M. L. Batari, M. N. Egbule and S. I. R. Okoduwa, *Clin. Nutr. Exp.*, 2019, **28**, 42–61.
33 L. L. Da Costa, T. J. Adorian, F. R. Goulart, J. Leitemperger, A. M. B. Do Amaral, V. L. Loro, S. S. Robalo and L. P. Da Silva, *Anim. Feed Sci. Technol.*, 2021, **276**, 114915.
34 S. M. Armah, *Int. J. Environ. Res. Public Health*, 2019, **16**, 1549.
35 X. Li, H. C. H. Lau and J. Yu, *Signal Transduction Targeted Ther.*, 2020, **5**, 211.
36 X. Ran, J. Liu, S. Fu, F. He, K. Li, G. Hu and W. Guo, *J. Agric. Food Chem.*, 2022, **70**, 381–391.
37 L. Zhang, Y. Wang, M. Yang, W. Yu, Z. Zhao and Y. Liu, *Polymers*, 2024, **16**, 1316.
38 X. Zhang, S. Zhang, X. Chen, Z. Ye, W. Liu, X. Liu and X. Wang, *Int. J. Biol. Macromol.*, 2024, **269**, 132080.
39 R. Wang, K. G. Neoh and E.-T. Kang, *J. Colloid Interface Sci.*, 2015, **438**, 138–148.
40 S. Yang, X. Tao, W. Chen, J. Mao, H. Luo, S. Lin, L. Zhang and J. Hao, *Adv. Mater.*, 2022, **34**, 2200693.
41 J. Zhang, Y. Hu, L. Zhang, J. Zhou and A. Lu, *Nano-Micro Lett.*, 2023, **15**, 8.
42 Y.-G. Ko, B. N. Kim, E. J. Kim, H. Y. Chung, S. Y. Park, Y.-J. Kim and O. H. Kwon, *Polymers*, 2022, **14**, 3909.
43 R. M. Cigala, F. Crea, G. Lando, D. Milea and S. Sammartano, *J. Chem. Thermodyn.*, 2010, **42**, 1393–1399.
44 T. U. Wani, A. H. Pandith and F. A. Sheikh, *J. Drug Delivery Sci. Technol.*, 2021, **65**, 102730.
45 Z. Wang, J. Xu, X. Wu, M. Han, R. Peng, R. Zhao, M. Qin, T. Li, J. Yin, L. Yu, Y. Li, H. Wu, Z. Lin, L. Wang, Y. Hu and Y. Wu, *Adv. Funct. Mater.*, 2024, 2408479, DOI: **10.1002/adfm.202408479**.
46 M. Li, K. G. Neoh, L. Q. Xu, R. Wang, E.-T. Kang, T. Lau, D. P. Olszyna and E. Chiong, *Langmuir*, 2012, **28**, 16408–16422.
47 V. Hoven, V. Tangpasuthadol, Y. Angkitpaiboon, N. Vallapa and S. Kiatkamjornwong, *Carbohydr. Polym.*, 2007, **68**, 44–53.
48 J. M. Banales, R. C. Huebert, T. Karlsen, M. Strazzabosco, N. F. LaRusso and G. J. Gores, *Nat. Rev. Gastroenterol. Hepatol.*, 2019, **16**, 269–281.
49 L. Campana, H. Esser, M. Huch and S. Forbes, *Nat. Rev. Mol. Cell Biol.*, 2021, **22**, 608–624.
50 S. Lorente, M. Hautefeuille and A. Sanchez-Cedillo, *Sci. Rep.*, 2020, **10**, 16194.
51 G. K. Michalopoulos and B. Bhushan, *Nat. Rev. Gastroenterol. Hepatol.*, 2021, **18**, 40–55.

